

DENSITIES OF STELLAR FLARES FROM SPECTRAL LINES

U. Mitra-Kraev ^a & J.-U. Ness ^{* b}

^aUniversity of Sheffield, Dept. of Applied Mathematics, Hicks Building, Sheffield S3 7RH, UK

^bArizona State University, Dept. of Physics and Astronomy, PO Box 871504, Tempe AZ 85287, USA

We present detailed analyses of spectral changes during X-ray flares. During flares the plasma is known to become hotter, but also changes in density are anticipated, as flares will rather be compact and dense than large and tenuous. We search for indications of changes in density in the spectra of *Chandra* High Energy Transmission Grating Spectrometer (HETGS) data. However, as flares usually last for at most up to one hour, only very bright flares will produce enough photons for a sufficiently well exposed spectrum. We chose long *Chandra* observations of flare stars which covered periods of time with flare activity that can be combined to compile one quiescent-only spectrum to be compared with a spectrum that is affected by flare activity. We show that with careful data analysis it is possible with the presently available instruments to detect spectral line changes between quiescent and flaring states, notably in the density- and temperature-sensitive lines of the He-like O VII-triplet (21.6/21.8/22.1 Å). Using cumulative distribution functions, we are also able to give solid statistical confidence limits. We also briefly discuss the diagnostic capabilities of other He-like line triplets and of observations carried out with the *XMM-Newton* Reflection Grating Spectrometer (RGS).

1. Introduction

Coronae of cool stars are likely to be highly structured similarly to the solar corona (see [1] for an extensive review on stellar X-ray coronae). During solar maximum loop structures of various intensities have been observed in soft X-rays, e.g., with *Yohkoh*. As the emission measure, proportional to the luminosity, is given by $EM = n_e n_p V$, where n_e and n_p are the electron and proton density and V the emitting volume, regions with high densities are brighter than those with low densities. The corona is dominated by the magnetic field, i.e., the magnetic pressure is much larger than the gas pressure, so that the ionised atmospheric particles are tied to the magnetic field lines.

While the solar disk can be observed in detail, stars are unresolved point sources. Any features in the stellar light curve or its spectrum are superpositions of all processes occurring on this star during that time. Flares, huge energy events which can dominate the light curve for a few minutes to several hours, are manifestations of the magnetic field reconnecting to a state of lower potential energy. In this process, the plasma is heated and fills post-flare loops and arcades. Measuring the density of a flare plasma and its corresponding emission measure enables

us to determine the emitting flare volume.

The multi-million degree hot stellar coronae and flares are bright in soft X-rays. The corresponding densities can be obtained from the density-sensitive lines in this spectral range, in particular from He-like transitions of C V, N VI, O VII, Ne IX, Mg XI and Si XIII [2,3]. The left panel of Fig. 1 depicts the relevant transitions. The upper level of the forbidden (*f*) line ($1s2s^3S_1$) has two major channels of transitions into other levels, either radiative decay into the ground state (with long decay times) or collisional excitation into the upper level of the intercombination line (*i*, $1s2p^3P_1$). With increasing density, the latter transition becomes increasingly important, thus leading to simultaneous reduction in *f*-line flux and increase in the *i*-line. The right panel of Fig. 1 shows the calculated density dependence of the *f*/*i* ratio for various ions using the CHIANTI database [4,5]. The temperature sensitivity ranges from $10^{6.9}$ K for the hottest ions (Si) to $10^{5.7}$ K for the cooler ones (N). The cooler ions are density-sensitive at lower densities, while the hotter ions probe only higher densities.

Chandra and *XMM-Newton* allow us to do time-resolved spectroscopy, as all observed X-ray photons are recorded in events files with their individual energy, detector position and arrival time. Therefore we can obtain spectra from any given combination of time intervals. In particu-

* *Chandra* fellow.

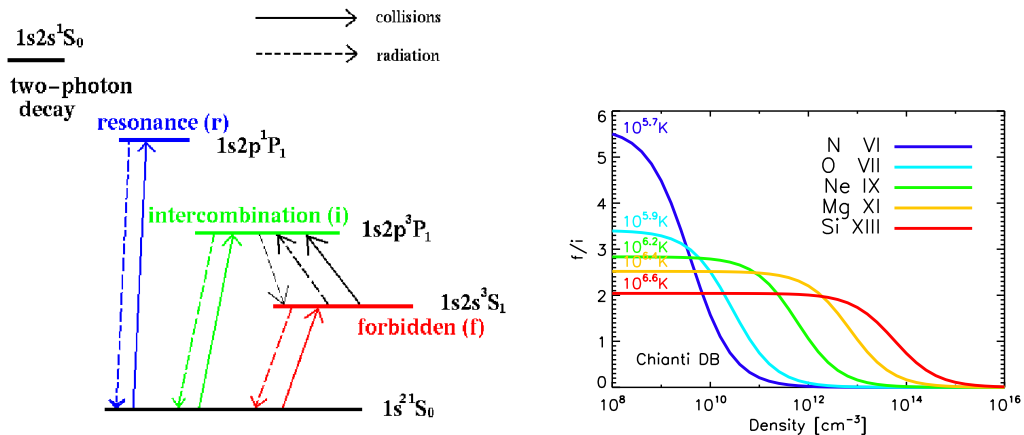


Figure 1. Left: He-like atomic transitions. Right: The f/i -ratio as a function of density for He-like ions at their respective maximum emission temperature.

lar, the light curve can be split into flaring and quiescent parts. Ideally, one would like to compare the spectrum of one flare (or a part thereof) to the quiescent state. However, this is only possible for very large flares with many recorded photons, where flare density increases derived from the O VII and Ne IX f/i ratio have been reported by [6–8]. More common are density comparisons between different stars [9–11]. Recently, [12] found spectral density variability in the corona of AD Leo between exposures taken several months apart.

We searched the *Chandra* archive for dMe flare stars for such spectral density increases (increases of the i line) between flaring and quiescent states. In Sect. 2 we present *Chandra* and *XMM-Newton* data of EV Lac. As we find strong indications for significant line changes of the i line of O VII for our discretionary chosen flare versus quiescent spectrum, which is contrary to what was reported by [13], we devised a bootstrap to estimate the statistical significance of the variations (Sect. 3). In Sect. 4 we present results from three other dMe stars, while a short discussion and conclusions are given in Sect. 5.

2. EV Lacertae

Figure 2 (left panel, top) shows the light curve of EV Lac observed with *Chandra*. It has a quiet (Q) phase during the first part of the observa-

tion and an active (A) phase during the second part, which makes it an ideal candidate to look for spectral changes between the two phases. We split the observation discretionary into a flaring (black) and quiescent (grey/blue) part, and reduce the spectrum of each. The top right panel of Fig. 2 shows the X-ray spectrum in the range of 21.4–22.2 Å, containing the He-like O VII line triplet, with the resonance line r at 21.6 Å, the intercombination line i at 21.8 Å, and the forbidden line f at 22.1 Å. The spectrum in black was obtained from the flaring phase of the observation and corresponds to the black part of the light curve, while the grey/blue part corresponds to the quiescent phase of the observation. The thickness of the spectral lines outlines the standard error, which roughly means that if the lines overlap there is no significant change in line intensity from one spectrum to the other, while if they are well separated, as is the case for the i line, the change is significant. The three oxygen lines are well separated, unblended and not affected by the flare continuum.

Table 1 gives our measurements of the density-dependent f/i ratio, the temperature-dependent $(f+i)/r$ ratio [3], and the temperature-dependent r/α ratio (the emission of the O VII resonance line divided by the O VIII Ly α line). There is a clear rise in density by a factor of 2. The flare temperatures however are not consistent. The temperature stays constant at 4 MK from the

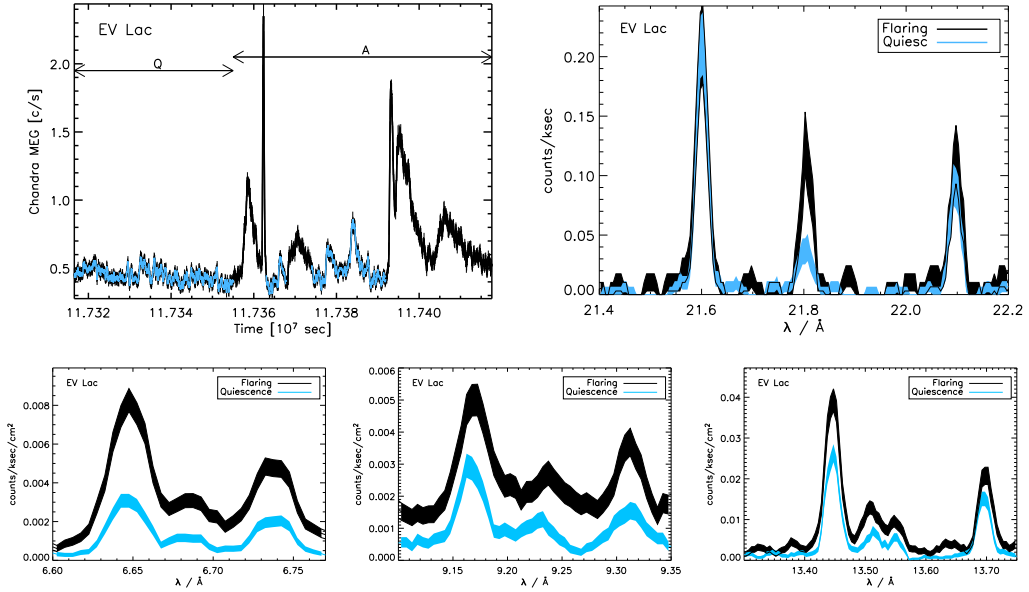


Figure 2. Top: Light curve and O VII spectrum and of EV Lac observed with *Chandra*. Bottom, from left to right: The corresponding Si XIII, Mg XI and Ne IX spectra.

r/α ratio, while it apparently decreases from the $(f+i)/r$ ratio. We will discuss this inconsistency in Sect. 5.

Table 1

EV Lac O VII rif and O VIII Ly α line ratios and derived electron densities and temperatures

	Quiet (Q)	Active (A)
f/i	1.7 ± 0.5	1.0 ± 0.2
$(f+i)/r$	0.6 ± 0.1	1.0 ± 0.2
r/α	0.19 ± 0.02	0.18 ± 0.03
n_e [10^{10}cm^{-3}]	5	10
$T_{(f+i)/r}$ [MK]	4	1.5
$T_{r/\alpha}$ [MK]	4	4

The bottom panels of Fig. 2 show the EV Lac flaring and quiescent flux spectra for Si XIII (6.6 – 6.8 Å), Mg XI (9.1 – 9.4 Å) and Ne IX (13.4 – 13.8 Å). Unlike the O VII triplet, the i line of neon is blended with iron lines, while the wings of the silicon and magnesium lines are overlapping and the flaring spectrum is at a higher flux

level due to the continuum radiation. Therefore we only concentrate on the oxygen lines in our further analysis.

Figure 3 shows EV Lac from the *XMM-Newton* observation, the light curves from the EPIC-pn (top) and RGS (bottom) instruments on the left, and the O VII spectrum in the right panel. Because of the lower spectral resolution of *XMM-Newton* RGS of $\Delta\lambda = 0.04$ Å compared to the spectral resolution of *Chandra* HETGS/MEG of $\Delta\lambda = 0.023$ Å (FWHM), the wings of the O VII triplet lines overlap and a spectral fit is more complicated. In the case of RGS the lines have to be fitted with line profiles in order to obtain line count rates, whereas in the case of HETGS/MEG the line count rates can be directly obtained by summation of all the counts within ± 0.05 Å around line centre.

3. Statistical assessment

How significant is the line change from the quiescent to the flaring spectrum of the O VII lines of the EV Lac *Chandra* observation? To answer this question we devise a bootstrap by reconstructing the cumulative distribution func-

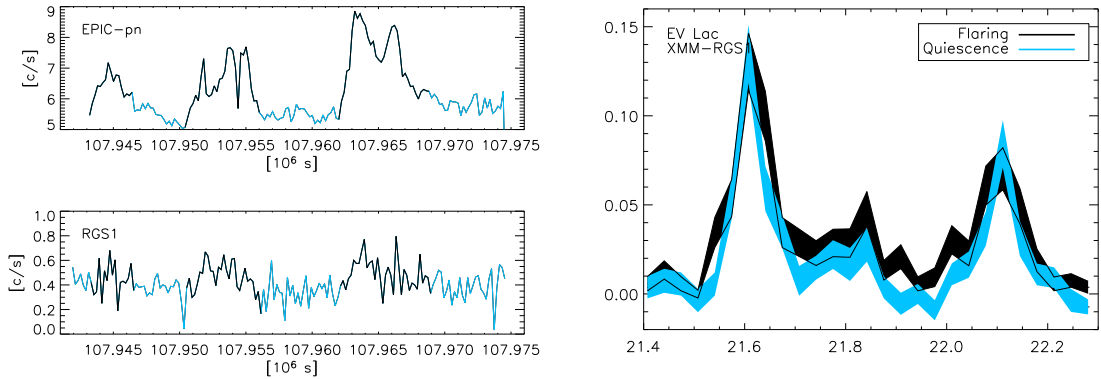


Figure 3. Light curve and O VII spectrum of EV Lac observed with *XMM-Newton*.

tion (CDF) for each line. The CDF is defined as $F(\Phi) \equiv \int_{-\infty}^{\Phi} f(\phi) d\phi$, where $f(\phi)$ is the normalised probability density function. Thus, F is an increasing function from 0 to 1 over $-\infty < \Phi < \infty$. Practically, we get the CDF by obtaining a large set of random variables (observations) Φ_n , with $n = 1, 2, \dots, N$ and N the number of elements in the set, so that the variables are sorted ($\Phi_{n+1} \geq \Phi_n$ for all n). For $\Phi_n \leq \Phi < \Phi_{n+1}$, the CDF is then given by $F(\Phi) = n/N$.

We obtain the CDFs by slicing the observation into 12 or less random, disjoint time intervals, then co-adding the photons of the even sections into one and the ones of the odd sections into the other spectrum, such that the two spectra add up to the total observation (each photon is associated with either one of the two spectra), and get the difference in the count-rate Δl for each spectral line we are interested in ($l = \alpha, r, i, f$), or, respectively, the count-rate excess of a line in units of its standard error ${}^l\Phi = \Delta l / \sigma_{\Delta l}$, with $\sigma_{\Delta l}$ the standard error of Δl . A value of ${}^l\Phi = 0$ means identical fluxes, a value of ${}^l\Phi = 1$ means that the lines differ with a significance of 1σ . This process of obtaining two random disjoint spectra is repeated 1000 times so that each ${}^l\Phi$ has $N = 1000$ elements.

The left panel of Fig. 4 shows the CDFs $F({}^i\Phi)$, $F({}^f\Phi)$, $F({}^r\Phi)$, and $F({}^\alpha\Phi)$ for the entire EV Lac observation. For comparison, the line between the shaded and the white area is the CDF of the normal distribution $\int_{-\infty}^{\Phi} \frac{1}{\sqrt{2\pi}} e^{-\frac{\phi^2}{2}} d\phi$. First, we notice that all the CDFs are symmetric around

$\Phi = 0$ and $F = \frac{1}{2}$, which confirms that our statistics is unbiased, as the ${}^l\Phi$'s are random and therefore have equal probability to be positive or negative. As the spectral noise is dominated by Poisson statistics, $F({}^l\Phi)$ is expected to follow the normal distribution if the line does not change intrinsically during the entire observation, but only fluctuates because of photon count uncertainty. This is the case for $F({}^r\Phi)$, meaning that the resonance line does not vary beyond flux uncertainty. The other CDFs, however, have a broader distribution. They vary more than just because of the photon count uncertainty, but because there is a real change in the physical conditions during the observation, i.e. density or temperature fluctuations. The crosses in the plot mark the values corresponding to the line excesses of the discretionary selected spectral pair displayed in Fig. 2.

The CDFs constructed from the entire observation do not allow us to answer the question whether the spectral variations are caused by the flares or not. To address this question, we make use of the fact that the light curve of EV Lac is neatly dividable into a quiet (Q) and an active (A) phase (see Fig. 2). Instead of dividing the entire observation randomly into two parts and taking the difference of the two spectra, we now take the difference between a random spectrum obtained during the active phase (a subset from the active phase) and a random spectrum from the quiet phase. The right panel of Fig. 4 shows the CDFs of the active versus quiet phase for our four spectral lines of interest, again in units of its

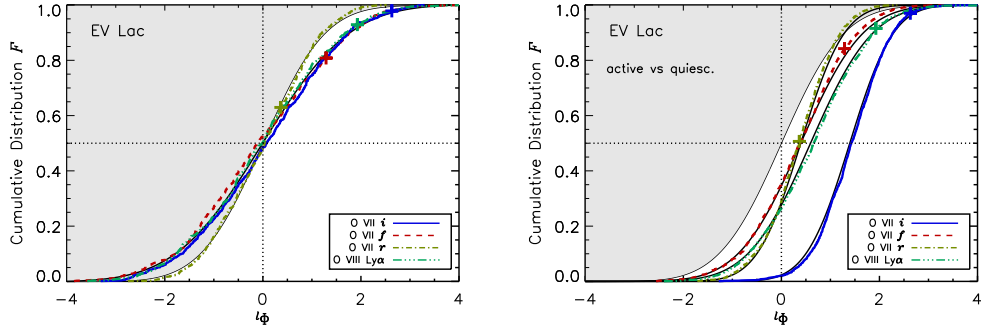


Figure 4. The CDFs for the entire EV Lac observation (left) as well as for the active versus quiet state on the right (see main text for more explanations).

standard error. The shift of all CDFs along the x-axis toward positive values reflects the general flux increase during the active phase compared with the quiet one. The r , f and α lines are shifted only very little, while the i line is shifted considerably toward larger values, implying a relative larger flux increase during flare activity for this line compared with the other ones. The confidence level for a line increase (where ${}^l\Phi > 0$) is 97% for the i line, but considerably smaller for the other lines (66% for f , 68% for r and 74% for α). Therefore we conclude that although the f as well as the α lines along with the i line show flux variations during the entire observation, the i line is the only one which is significantly enhanced during flares.

4. AD Leonis, Proxima Centauri and AU Microscopii

Can we also observe temporal variations of the investigated oxygen lines in other flare stars? We analysed the data of AD Leo, Proxima Cen and AU Mic, all active M-type dwarfs like EV Lac which were also observed by *Chandra* HETGS. Figure 5 shows the light curves (left panels), the spectral regions around O VII and OVIII (middle panels) and the CDFs (right panels) of AD Leo, Proxima Cen and AU Mic (from top to bottom). AD Leo and AU Mic have many small flares or fluctuations comparable to the small variations during the quiescent phase of the EV Lac observation, where the flux level changes by less than a factor of 2. In comparison, the flux changed by

up to a factor of 4 during the flares of EV Lac. These ongoing small variations make it impossible to split the observation into two different activity stages like we did for EV Lac, thus we can only investigate the statistical behaviour of the total observation, but are not able to make a comparison between two different phases. Proxima Cen has a flare at the beginning of the observation with a flux increase by a factor of approximately 3 and thereafter stays at a very low emission level. The flux level of the quiescent phase of Proxima Cen is at about half the level of any of the other quiet emission levels. Therefore, the signal-to-noise ratio is rather poor, which is reflected in the weak lines and large error regions of the spectrum. By eye, none of the oxygen emission lines of these three stars varies significantly between the pairing two spectra, except for the O VIII Ly α line of Proxima Cen, which is because of the larger flux and suggests a higher temperature during the flare. All the CDFs except the one for the O VIII Ly α line of Proxima Cen are close to normally distributed. The latter reflects the temperature increase of the Proxima Cen flare.

5. Discussion and conclusions

We find that the intercombination line flux of O VII increases significantly during flares on EV Lac, while the other O VII line fluxes remain unchanged. This suggests increased densities (from 5 to $10 \cdot 10^{10} \text{ cm}^{-3}$) during flares at 4 MK. However, this rise is only in the intercombination line and not in the resonance or the forbidden line

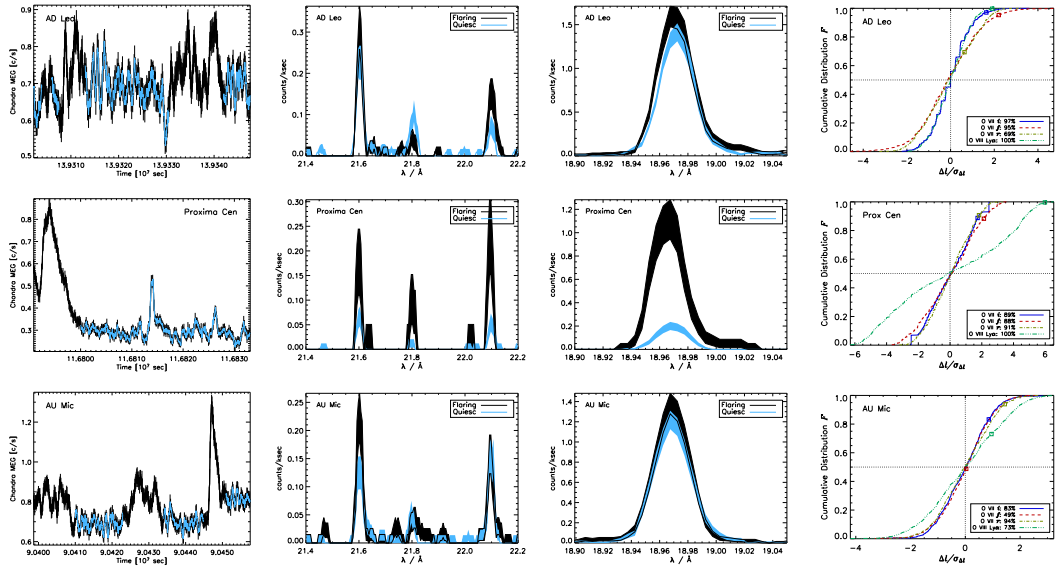


Figure 5. Light curves, O VII and O VIII spectra and CDFs for AD Leo, Proxima Cen and AU Mic.

would yield to a lower flare temperature under the assumption of collisionally ionised plasma, which is not supported by the temperature derived from the O VII/O VIII ratio. One possible solution to this conundrum is that photons which should be in the resonance line are resonantly scattered out of the line-of-sight during the flares, which is possible depending on flare geometry. However, other ratios (of Fe XVII lines) which would be affected by resonance scattering are not changed between quiescent and flaring state in this observation, so the resonance scattering hypothesis has to be rejected. We suggest that the suppressed resonance flux along with the increased flux in the intercombination line during the flares could be due to a recombining photoionised plasma [14], as is the case for cooling plasmas in non-thermal environments, which might be supported by recent radiative hydrodynamic models of M dwarf flares [15].

REFERENCES

1. Güdel, M. 2004, A&A Rev., 12, 71.
2. Gabriel, A.H. & Jordan, C. 1969, MNRAS, 145, 241.
3. Porquet, D., Mewe, R., Dubau, J. *et al.* 2001, A&A, 376, 1113.
4. Dere, K.P. *et al.* 1997, A&AS, 125, 149.

5. Landi, E. *et al.* 2006, ApJS, 162, 261.
6. Güdel, M., Audard, M., Skinner, S.L., & Horvath, I. 2002, ApJ, 580, L73.
7. Raassen, A.J.J., Mewe, R., Audard, M., & Güdel, M. 2003, A&A, 411, 509.
8. van den Besselaar, E.J.M., Raassen, A.J.J., Mewe, R. *et al.* 2003, A&A, 411, 587.
9. Ness, J.-U., Mewe, R., Schmitt, J.H.M.M. *et al.* 2001, A&A, 367, 282.
10. Ness, J.-U., Schmitt, J.H.M.M., Burwitz, V. *et al.* 2002, A&A, 394, 911.
11. Testa, P., Drake, J. J., & Peres, G. 2004, ApJ, 617, 508.
12. Maggio, A., & Ness, J.-U. 2005, ApJ, 622, L57.
13. Osten, R.A., Hawley, S.L., Allred, J.C. *et al.* 2005, ApJ, 621, 398.
14. Pradhan, A.K. 1985, ApJ, 288, 824.
15. Allred, J.C., Hawley, S.L., Abbett, W.P., & Carlsson, M. 2006, astro-ph/0603195.

ACKNOWLEDGEMENTS

UMK acknowledges financial support from the UK Particle Physics and Astronomy Research Council. JUN gratefully acknowledges support provided by NASA through Chandra Postdoctoral Fellowship grant PF5-60039 awarded by the Chandra X-ray Center, which is operated by the Smithsonian Astrophysical Observatory for NASA under contract NAS8-03060.